International Journal of CAD/CAM Vol. 3, No. 1, pp. 1~12 (2003)

INTERNATIONAL JOURNAL OF CAD/CAM
www.ijcc.org

Modeling Cutter Swept Angle at Cornering Cut

H.S. Choy* **and K.W. Chan**
Department of Mechanical Engineering, The University of Hong Kong, Pokfulam, Hong Kong

Abstract – When milling concave corners, cutter load increases momentarily and fluctuates severely due to concentration and uneven distribution of material stock. This abrupt change of cutter load produces undesirable machining results such as wavy machined surface and cutter breakage. An important factor for studying cutter load in 2.5D pocket milling is the instantaneous Radial Depth of Cut (RDC). However, previous work on RDC under different corner-cutting conditions is lacking. In this paper, we overview typical work done by other researchers on cornering cut, followed by presenting our study on RDC for different corner shapes. In our work, we express RDC mathematically in terms of the instantaneous cutter engage angle which is defined as Cutter Swept Angle (CSA). An analytical approach for modeling CSA is explained. Finally, examples are shown to demonstrate that the proposed CSA modeling method can give an accurate prediction of cutter load pattern at cornering cut.

Keywords: **Pocket milling, concerning cut, cutter load, tool path, machining**

1. Introduction

Pocket milling is a metal removal operation commonly used for creating depressions in machined parts. Generating tool path for milling a pocket begins by slicing the pocket into a number of horizontal layers. The layer gap width represents the incremental depth of cut along the spindle or cutter axis. The pocket boundary of each layer is revealed by evaluating the curves formed between the intersection of the dissecting plane and the pocket's wall faces. Using the determined pocket boundary of each layer, different tool path patterns can then be employed to remove the stock material within the pocket region.

Popular pocket milling tool path patterns provided by contemporary CAM systems are zig, zig-zag and contour-parallel offset (CPO) as illustrated in Fig. 1. Among these three patterns, CPO tool path is most widely adopted because it produces lesser idle tool path portions and can maintain a consistent use of down-cut (or up-cut) milling method. However, CPO tool path inherently produces many convex and concave corners.

Before addressing the cutter problems caused by corners, it is necessary to introduce a measure for cutter load or chip load. As mentioned by Kline *et al.* [6], cutter load is directly related with chip thickness as shown in Fig. 2 where chip thickness is defined to be the distance between previously machined boundary and currently machined boundary. It is the maximum thickness of material in the radial direction that a cutting edge encounters and is important in assessing cutter load on the edge. However, chip thickness is also directly related with the cutter engage arc length. As an example, the cutter engage arc length for a cutter of diameter 20 mm is divided into 10 equal portions, which represents different stepover distances shown in Figs.

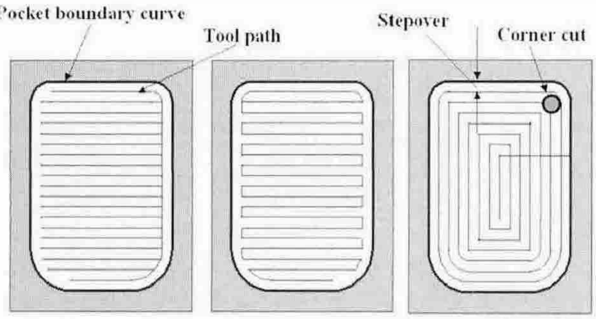

(a) zig cut (b) Zigzag cut (c) Contour-parallel cut

Fig. 1. Three commonly used tool path patterns.

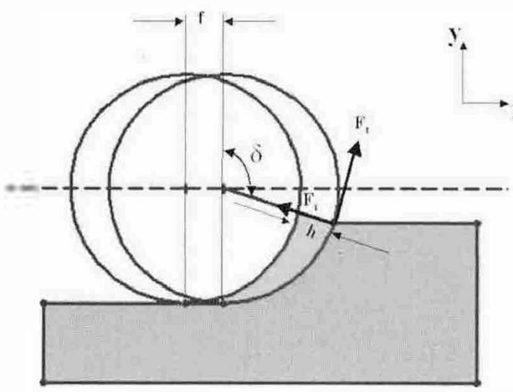

where f = Feed distance, F_r = Radial cutting force, F_t = Tangential cutting force, h = Chip thickness, δ = An angle for controlling stepover distance.

Fig. 2. Classical cutting force estimation.

*Corresponding author:
Tel: +852-2859-2642
Fax: +852-2858-5415
E-mail: hangshan@hkem.com

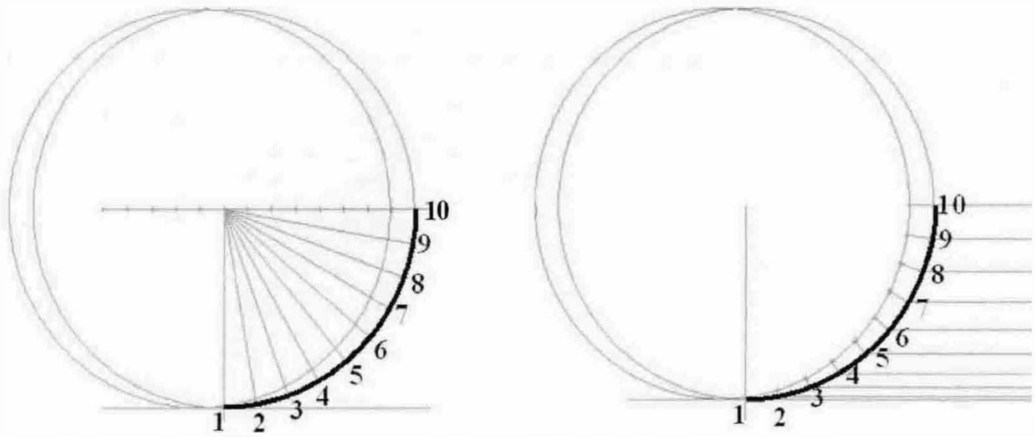

(a) Division of cutter engage arc lenght (b) Different chip thickness for different stepover distance

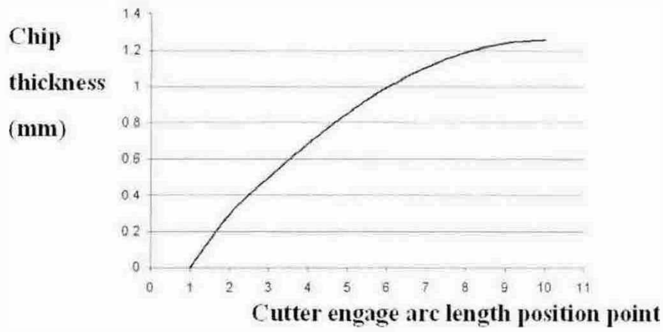

(c) Chip thickness calculated for different cutter engage arc length

Fig. 3. Relation between chip thickness and cutter engage arc length.

3(a) and (b). The corresponding chip thickness for different cutter engage arc lengths is plotted in Fig. 3(c) under a specified feed distance of 1.23 mm. It can be observed that the cutter engage arc length is directly proportional to the chip thickness. Therefore, it can be deduced that cutter engage arc length can also be used for estimating cutter load.

The corner cutting problems are now illustrated as follows: By referring to Fig. 4, it can be easily observed that when a cutter moves from a linear tool path segment into a convex corner, the cutter engage arc length effectively decreases. This means that cutter load will drop when performing convex cornering cut. This also implies that convex corners create less problem to machining since the change of chip load involved is a decrease rather than an increase. As an example, the cutting result for line-line and line-arc-line convex corners is selected to illustrate the difference between their encountered cutting forces. Shown in Fig. 5(a)-(f) is the cutting forces encountered by a cutter of diameter 10 mm for different corner tool path radii are. When the cutter approaches the corner region, the cutting force encountered shown in Fig. 5(f) is substantially dropped close to zero. It means there is a short period of idle cutting time. Therefore, a convex corner will not lead to a harmful cutting problem such

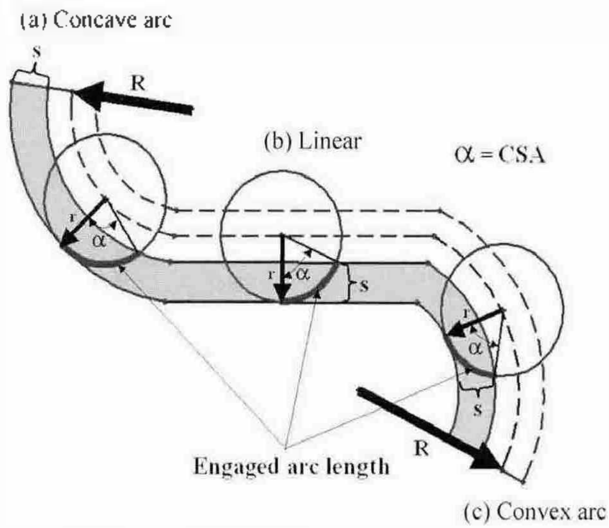

Fig. 4. Cutting path classification.

as cutter deflection or even cutter breakage. However, the convex corner has the problem of having idle cutting tool path portions shown in Fig. 6(a). A special tool path construction should be used for minimizing the problem such that the offset segments at convex corners will be extended and connected by adding circular arcs in Fig. 6(b). If the tool path for convex corners is offset

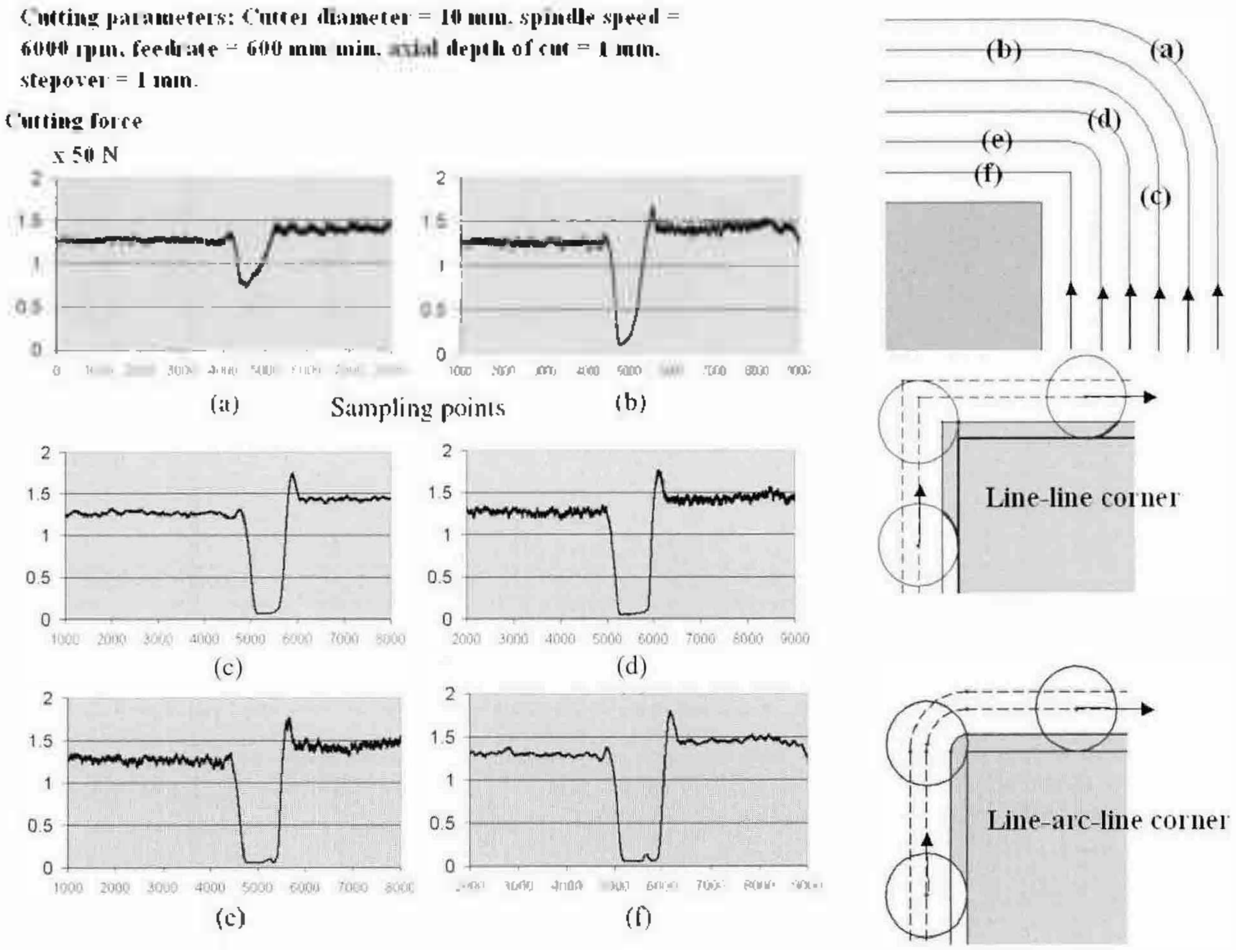

Fig. 5. Experimental result for convex corner.

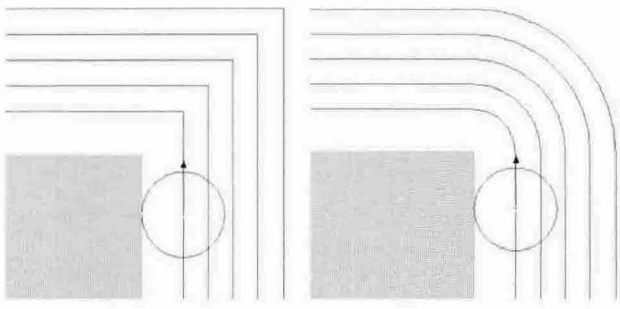

(a) Conventional method (b) Improved method

Fig. 6. Tool path construction for convex corner.

by means of the mentioned approach, the problem of idle cutting tool path portions can be solved substantially. The larger the fillet radius at convex corner tool path, the more effective for solving the idle cutting time problem as shown in Fig. 5(a).

On the contrary, when a cutter moves from a linear tool path segment into a concave corner, the cutter engage arc length rises quickly, achieving a maximum value at the middle part of the corner, and then decreases as the cutter leaves the corner. Such a sharp rise and fall of cutter engage arc length at concave corners will lead to undesirable results such as machine vibration, chatter marks on machined surface and even tool breakage when the cutter load is excessive. To avoid these adverse consequences, machining practitioners usually resort to using a lower cutting feedrate and or depth of cut which leads to a reduction of machining efficiency. Maintaining a high machining efficiency, however, is of paramount importance for increasing competitiveness amidst today's stringent market conditions. Motivated by these background reasons, we therefore conducted an in-depth investigation on concave cornering cut and reported our findings in this paper.

The remainder of this paper is organized as follow. Section 2 overviews previous work on cornering cut. Section 3 describes CSA for different corner cases in detail. The formation of different CSA zones is explained with illustrations and the determination of the CSA values in different zones is expressed mathematically. Examples are given and compared for different approaches in sections 4. Section 5 concludes our work.

2. Review of previous work

In earlier work, Kline *et al.* [6] used a mechanistic model to estimate chip load and found that there was a dramatic change in cutting force at cornering cut. Iwabe *et al.* [5] established a geometry analysis of the interaction between an end mill cutter and an inside corner. Tlusty *et al.* [11] proved that the change in radial depth of cut at corner had an adverse effect on machining stability such as causing high frequency chatters.

Two major approaches can be identified for tackling cornering cut problem, namely the adaptive control and the modification of tool path geometry. The former approach focuses on controlling the cutting performance by adjusting the cutting parameters instantaneously during cutting. For instance, Tarng *et al.* [10] attempted to maintain a constant metal removal rate in pocket milling by adjusting feedrate adaptively. Spence *et al.* [8] scheduled the feedrate automatically so as to satisfy force, torque, and dimensional error constraints. Fussell *et al.* [2] used a feedrate planning system to select feedrate for 3-axis sculpture milling by integrating a Z-buffer geometric model with a discrete mechanistic model of the cutter. A pre-requisite for applying this approach is a sophisticated NC machine that possesses NC program look-ahead function for advanced calculation of cutting conditions and a rapid acceleration/deceleration control mechanism to response to the frequent and quick change of feedrate.

The latter approach aims to adjust the chip load by using special tool path trajectory. For example, Tsai *et al.* [12] modified CPO tool path segments in order to reduce corner cutting problems such as chatter vibration and excessive machining errors. Stori *et al.* [9] presented a constant cutter engagement tool path for reducing cutting force variation at corner cutting. However, their spiraling tool path can only be applied to a limited set of corner shapes.

Hinduja *et al.* [3] applied 2-D union operation to combine the area swept by the bottom face of an end mill and the remaining stock area left over by the previous machining path for finding RDC variation. More recently, they [4] also reported the application of RDC variation to selecting optimum cutter diameter for pocket machining. However, their approximate approach for finding the instantaneous RDC cannot handle more complicated corner shapes that were defined by Choy *et al.* [1].

The static cutter engage angle along line and arc segments was formally defined by Kramer [7]. However, the continuous dynamic change of cutter engage angle at concave corners has not been addressed in his work. Instead of simply using the static cutter engage angle or RDC, we consider that the instantaneous cutter swept angle CSA is a more appropriate parameter to describe the corner cutting condition because CSA can be used to describe the different stages of cutter engage angle change during a cornering cut. We are also not aware of any previous research work done on CSA for complicated concave corners that are formed by different boundary geometries. Our work therefore focuses on modeling CSA at cornering cut for complicated corner shapes.

3. Analytical representation of CSA

We focus our consideration on pocket milling tool paths that are formed by line, concave and convex arc segments. Referring to Fig. 4, the governing equations of CSA, α, for these three basic tool path geometries are:

Linear	$\cos(\alpha)=1-s/r$	(1)
Concave arc	$\cos(\alpha)=1-s/r-\Gamma$	(2)
Convex arc	$\cos(\alpha)=1-s/r+\Gamma$	(3)

where $\Gamma=s(r-0.5s)/(Rr)$, and s, r and R are the stepover distance, cutter radius and circular cutting path radius respectively. It can be observed that $\Gamma\geq 0$ since $2r\geq s$, and α decreases as s decreases.

Moreover, different cutting modes can be discerned by the following rules:

If CSA = 180°, the cutter is performing a slot cutting operation,

If 90 < CSA < 180°, the cutter is subject to both up-cutting force on one side and down-cutting force on another side,

If CSA ≤ 90°, there are two possible cases. Case 1: The cutter is performing up-cutting. This case occurs when the table feeds the workpiece in the opposite direction to the cutter rotation as shown in Fig. 7(a). The chip formation begins from nil to a maximum thickness as the tooth leaves the workpiece. Case 2: The cutter is performing down-cutting. This case occurs when the table feeds the workpiece in the same direction as the cutter rotation as shown in Fig. 7(b). The chip thickness is maximum at the beginning and gradually reduces to nil as the cutter exits the material.

An arc segment can be classified as either clockwise (CW) or counterclockwise (CCW) depending on its traversal direction with respect to the starting point S and ending point E (Fig. 8). Based on the possible connection of the tool path entity and their traversal order of the three basic types of tool path geometry (Fig. 8), nine different corner types can be formed as

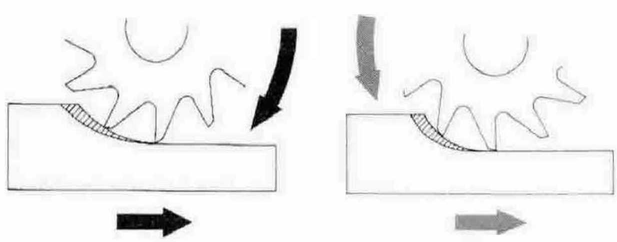

(a) Up cut (b) Down cut

Fig. 7. Up cut and down cut operations.

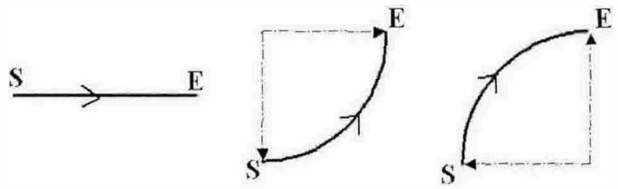

(a) Line (b) CCW Arc (c) CW Arc

Fig. 8. Tool path geometries.

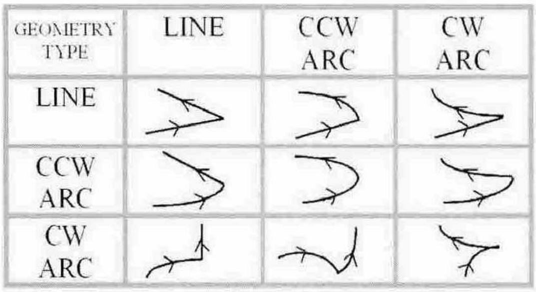

Fig. 9. Different corner types.

shown in Fig. 9.

As mentioned in section 1 and judged from equation 3, convex corners do not introduce drastic rise of chip load problem. Hence only concave corners are considered. Besides corner shape, the geometry of the previous and current tool paths also affects the corner cutting conditions significantly because the remaining stock material is governed by the geometry of the previous tool path. We therefore studied the following three tool path cases for deriving the expression of CSA in concave corner region.

3.1. Classification of corner cases

Based on the geometric configuration of the previous and current tool centre paths, three different corner cases can be identified:

Case 1: Both previous and current tool centre paths have no joining fillet at corner (Fig. 10(i)).
Case 2: Previous tool centre path has no joining fillet but current tool centre path has joining fillet at corner (Fig. 10(ii)), and
Case 3: Both previous and current tool centre paths have joining fillets at corner (Fig. 10(iii)).

· Case 1: This case occurs when the cutter radius is smaller than or equal to the corner radius of the pocket. Nine possible corner shapes for this case are shown in Fig. 11(i). For explanation purpose, the case shown in Fig. 11(i) (a) is used. From the enlarged view shown in Fig. 12, it can be seen that the previous tool centre path is indicated by segments AB and BC while the current tool centre path is shown by segments DE and EF. Segments GH, HI and IJ represent the remaining stock boundary swept by the cutter when the cutter centre moves along the previous tool center path. Two intermediate points of interest, D_1 and E_1, are introduced in the figure. Point D_1 lies on DE and represents the particular cutter centre position when the cutter boundary intersects point H which is created by a perpendicular projection from point B to GH. Similarly, point E_1 lies on EF such that the cutter boundary intersects point I which is formed by projecting a line perpendicularly from point B to IJ.

· Case 2: This case occurs when the cutter radius is much smaller than the corner radius of the pocket. Nine possible corner shapes for this case are displayed in Fig. 11(ii). The case shown in Fig. 11(ii) (a) is enlarged in Fig. 13 for the following explanation. Segments AB and BC represent the previous tool centre path while segments DE, EF and FG display the current tool centre path. Segments HI, IJ and JK represent the remaining stock boundary swept by the cutter when the cutter centre moves along the previous tool center path. Point D_1 lies on DE and represents the particular cutter center position when the cutter boundary intersects

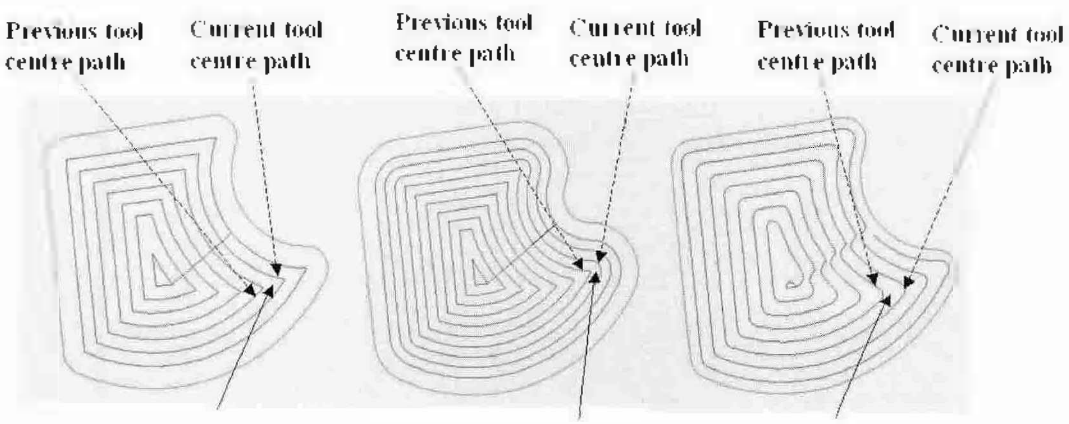

(i) Case 1 (ii) Case 2 (iii) Case 3

Fig. 10. Possible corner cases.

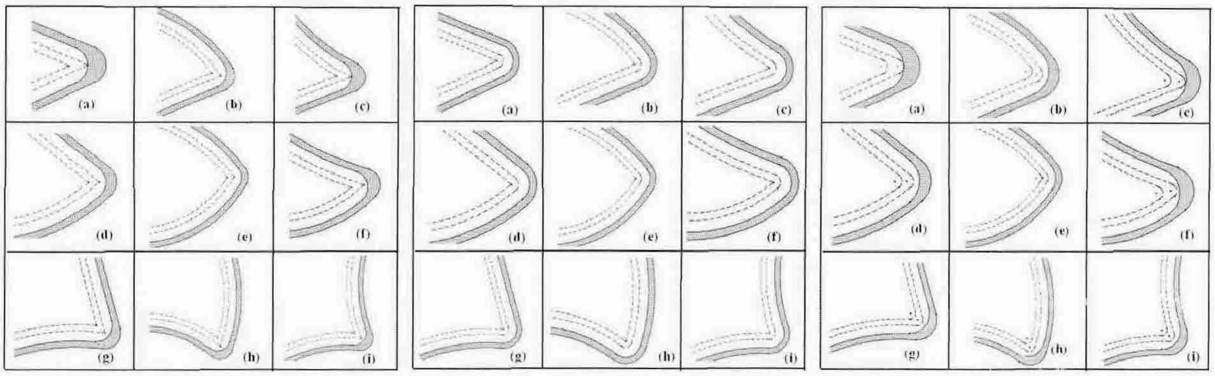

(i) Case 1 (ii) Case2 (iii) Case3

Fig. 11. Nine possible corner shapes for each of the three cases.

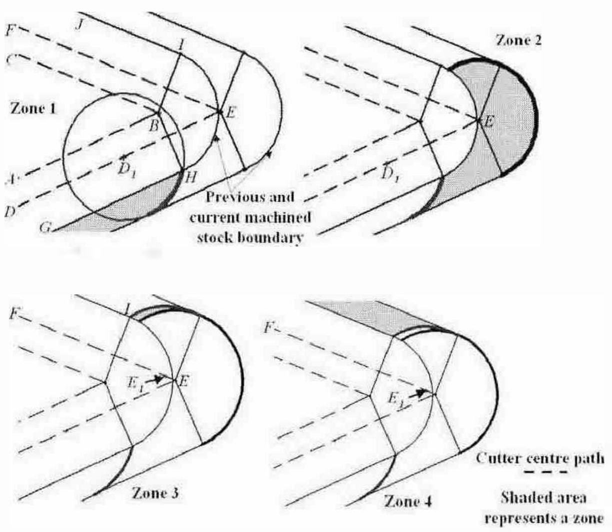

Fig. 12. Different CSA zones for case 1.

point I. Point I is made by the perpendicular projection from point B to HI. Similarly, point E_1 lies on EF such that the cutter boundary intersects point J which is made by a line normally projected from point B to JK.

· Case 3: This case occurs when both the previous and current tool centre paths have a specified fillet radius. Nine possible corner shapes for this case are depicted in Fig. 11(iii). Fig. 14 shows the enlarged view of the first case shown in Fig. 11(iii) (a) for explanation purpose. Segments AB, BC and CD show the previous tool centre paths while segments EF, FG and GH illustrate the current tool centre paths. Segments IJ, JK and KL represent the remaining stock boundary swept by the cutter when the cutter centre moves along the previous tool center path. Point E_1 lies on EF and indicates the particular cutter centre position when the cutter boundary intersects point J. Point J is made by the perpendicular projection from point O to IJ. Similarly, point G_1 lies on GH and represents the cutter centre position when the cutter boundary intersects point K which is created by projecting a perpendicular line from point O to KL.

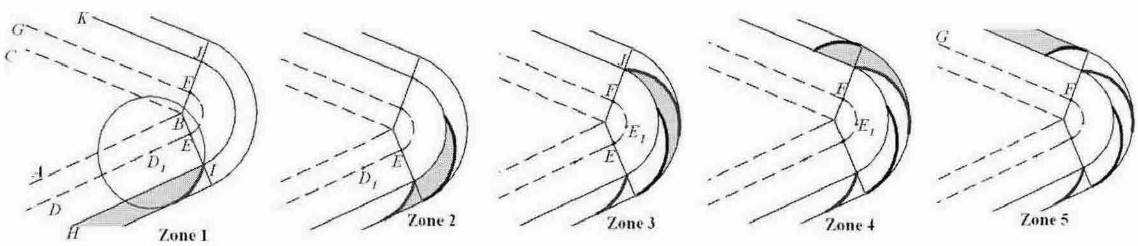

Fig. 13. Different CSA zones for case 2.

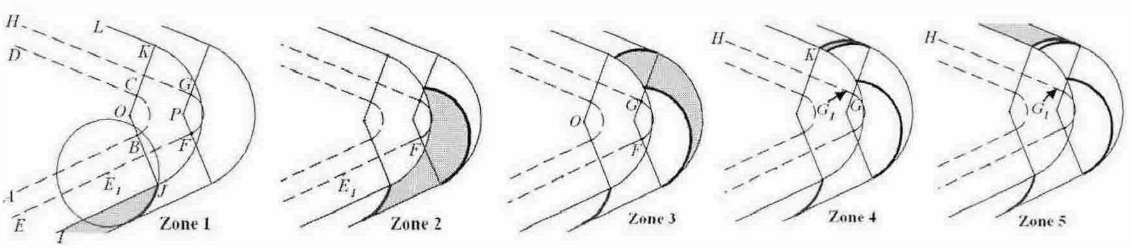

Fig. 14. Different CSA zones for case 3.

3.2. Defining different CSA zones

According to the identified corner cases, the cutting stages for each corner case were scrutinized and different zones of CSA for the three exemplary corner cases were defined below.

Case 1: Four CSA zones as shown by the shaded regions in Fig. 12 can be defined and summarized in Table 1.

Case 2: Five CSA zones as shown by the shaded regions in Fig. 13 can be defined and summarized in Table 2.

Case 3: Five CSA zones as shown by the shaded regions in Fig. 14 can be defined and summarized in Table 3.

3.3. Special CSA calculation procedures

Determination of the CSA values for some portions of the corner tool path segments mentioned above

Table 1. Scrutiny of CSA zones for case 1

Zone	Description	Value of CSA	Determination of CSA value
1	Corresponds to the region machined when the cutter centre moves from points D to D_1.	Constant	If DD_1 is a line, determine by equation (1), else if DD_1 is a CCW arc, determine by equation (2), else DD_1 is a CW arc, determine by equation (3).
2	Corresponds to the region machined when the cutter centre moves from points D_1 to E.	Varying	By the special procedure described in section 3.3.1
3	Corresponds to the region machined when the cutter centre moves from points E to E_1.	Varying	By the special procedure described in section 3.3.1
4	Corresponds to the region machined when the cutter centre moves from points E_1 to F.	Constant	If E_1F is a line, determine by equation (1), else if E_1F is a CCW arc, determine by equation (2), else E_1F is a CW arc, determine by equation (3).

Table 2. Scrutiny of CSA zones for case 2

Zone	Description	Value of CSA	Determination of CSA value
1	Corresponds to the region machined when the cutter centre moves from points D to D_1.	Constant	If DD_1 is a line, determine by equation (1), else if DD_1 is a CCW arc, determine by equation (2), else DD_1 is a CW arc, determine by equation (3).
2	Corresponds to the region machined when the cutter centre moves from points D_1 to E.	Varying	By the special procedure described in section 3.3.1
3	Corresponds to the region machined when the cutter centre moves from points E to E_1.	Constant	By equation (2) because the cutter is basically cutting along a CCW arc.
4	Corresponds to the region machined when the cutter centre moves from points E_1 to F.	Varying	If JK is a line, determine by the special procedure described in section 3.3.2. Otherwise, determine by the special procedure described in section 3.3.1.
5	Corresponds to the region machined when the cutter centre moves from points F to G.	Constant	If FG is a line, determine by equation (1), else if FG is a CCW arc, determine by equation (2), else FG is a CW arc, determine by equation (3).

Table 3. Scrutiny of CSA zones for case 3

Zone	Description	Value of CSA	Determination of CSA value
1	Corresponds to the region machined when the cutter centre moves from points E to E_1.	constant	If EE_1 is a line, determine by equation (1), else if EE_1 is a CCW arc, determine by equation (2), else EE_1 is a CW arc, determine by equation (3).
2	Corresponds to the region machined when the cutter centre moves from points E_1 to F.	Varying	By the special procedure described in section 3.3.1
3	Corresponds to the region machined when the cutter centre moves from points F to G.	Varying	By the special procedure described in section 3.3.1
4	Corresponds to the region machined when the cutter centre moves from points G to G_1.	Varying	By the special procedure described in section 3.3.1
5	Corresponds to the region machined when the cutter centre moves from points G_1 to H.	constant	If G_1H is a line, determine by equation (1), else if G_1H is a CCW arc, determine by equation (2), else G_1H is a CW arc, determine by equation (3).

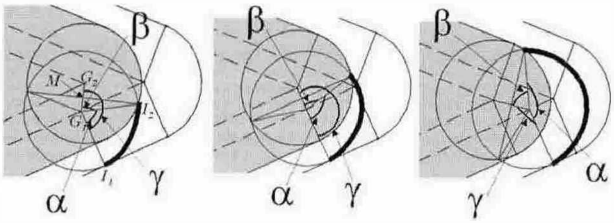

Fig. 15. CSA for two circle case.

requires more detailed analysis.

Let point I_1 be the intersection point made between the cutter boundary and the currently machined stock boundary as shown in Fig. 15, and point I_2 be the intersection point made between the cutter boundary and the previously machined stock boundary. It can be observed that if points I_1 and I_2 are found, CSA can be determined simply by using cosine rule.

Point I_1 can be determined easily by projecting a line from the current cutter center location G_1, normal to the current tool centre path segment and intersecting the currently machined stock boundary.

However, since point I_2 can be formed by two possible cases: 1) intersection between two circles (i.e. current cutter boundary intersects an arc segment in previously machined stock boundary) or 2) intersection between a line and a circle (i.e. current cutter boundary intersects a line segment in previously machined stock boundary), its determination requires the following two different sets of procedures.

3.3.1. Intersection of two circles case

Consider two circles shown in Figs. 15 and 16 with centers G_1 and G_2 and radii r_1 and r_2 respectively. Let M be the intersection point made between the line G_1G_2 and the common chord of the two circles.

Let γ be the included angle between line G_1I_1 and line G_1G_2, and β be the included angle between line G_1I_2 and line G_1G_2. The CSA, represented by α, can be determined by

Case A(Fig. 15(a)): If G_1G_2 has not been parallel to G_1I_1 when the cutter entering the corner, $\alpha = \gamma - \beta$.

Case B(Fig. 15(b)): If G_1G_2 is parallel to G_1I_1 when the cutter entering the corner, $\gamma = 180$ degrees and $\alpha = \gamma - \beta$.

Case C(Fig. 15(c)): If G_1G_2 has once been parallel to G_1I_1 when the cutter entering the corner, $\alpha = 360° - (\gamma + \beta)$.

γ is determined by the equation:

$\cos(\gamma) = \langle G_1I_1 \cdot G_1G_2 \rangle / (|G_1I_1|\ |G_1G_2|)$ where $\langle \cdot \rangle$ and $||$ are dot product and magnitude operator respectively. G_1I_1 is the line vector from point G_1 to point I_1. Similarly, G_1G_2 is the line vector from point G_1 to point G_2.

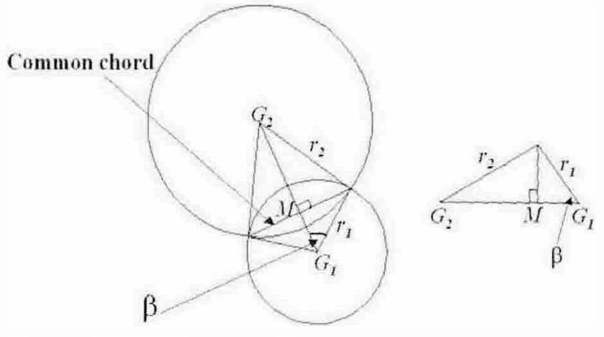

Fig. 16. Circles with different radii.

β can be determined by the following rule

If $r_1 = r_2$ (this means the two circles have equal diameters)

then $\cos(\beta) = |MG_1| / r_1$ (or $\cos(\beta) = |MG_2| / r_2$) where point M lies on the mid-point of G_1G_2.

else if $r_1 \neq r_2$ (this means the two circles have unequal diameters as shown in Fig. 16)

then $\cos(\beta) = \{(G_1G_2)^2 + (r_1)^2 - (r_2)^2\} / 2(G_1G_2)(r_1)$

3.3.2. Intersection of a line and a circle case

Consider a circle of radius r with center $G(x_c, y_c)$ and a line L_2 with equation $a.x + b.y + c = 0$ shown in Fig. 17. Let point S be the closest distance point between circle center G and line L_2, β be included angle between line GI_2 and line GS, γ be the included angle between line GS and GI_1. Hence, it can be observed that $\alpha = \gamma + \beta$.

β can be determined by $\cos(\beta) = |GS| / r$ where $||$ is the magnitude operator and $|GS|$ = the absolute value of $((a.xc + b.yc + c) / \sqrt{a^2 + b^2})$, a, b and c are the coefficients of line L_2. The calculation of distance GS is obtained by considering the normal distance of the point G from the line L_2.

γ can be determined by $\tan(\gamma) = (m_2 - m_1)/(1 + m_1 \cdot m_2)$ where m_1 is the slope of the line I_1G and m_2 is the slope of a line normal to line L_2.

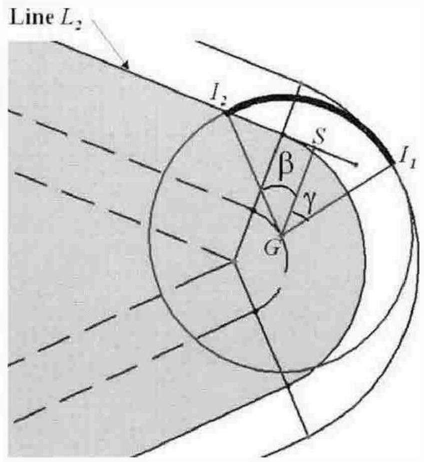

Fig. 17. CSA for a line and a circle case.

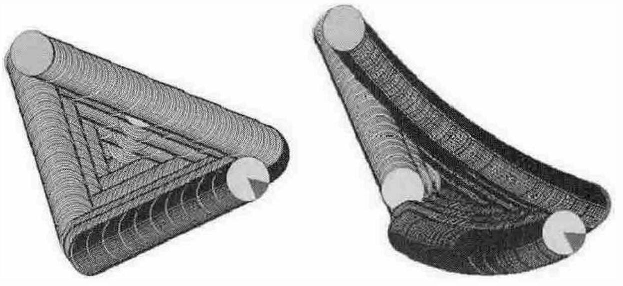

(a) Line-line corner case (b) CCW arc-CW arc corner case

Fig. 18. Modeling the cutter swept angle for 2 corner cases.

If the calculated α in sections 3.3.1. or 3.3.2. is greater than 180 degrees, α will be automatically set to 180 degrees since this is not the maximum possible CSA, indicating that the cutter is performing a slot cutting operation.

3.4. Plotting the change of CSA (Fig. 18(a))

The calculated CSA values for the exemplary corners shown in Figs. 12, 13 and 14 are plotted graphically in Figs. 19(a), (b) and (c) respectively. The corner angle and stepover distance for Figs. 12, 13 and 14 are the same. The corner angle and cutter diameter are 46 degrees and 10 mm respectively. The stepover distance and fillet radius used are both 2 mm.

4. Discussion of results

It can be seen from Fig. 19(a) that as the cutter moves from the linear tool path into the corner, the CSA rises very rapidly, reaching a maximum of 180° at the middle part of the corner, and then falls off vertically as the cutter leaves the corner. This vividly shows that without round fillets added to the tool centre paths, the chip load at cornering cut will increase momentarily as indicated by the sharp "spike" shape of the CSA plot. This will produce adverse machining results and even tool breakage especially when performing high speed machining.

Fig. 19(b) represents the case that a circular fillet has been introduced to the current tool centre path. Since there is no fillet in the previous tool centre path, the stock material left behind for the current filleted tool path to remove is effectively less. Hence, the rise of CSA in zone 2 is less rapid. Most importantly, there is a stable zone 3 in which the maximum CSA value is significantly reduced to about 100°. The decrease of the CSA value in zone 4 is also more gentle. Comparing with the plot in Fig. 19(a), it can be seen that the middle part shape of the CSA plot in Fig. 19(b) has been stretched horizontally. This indicates a beneficial effect as it implies that the chip load during corner cutting can be suppressed and maintained more steady in this case.

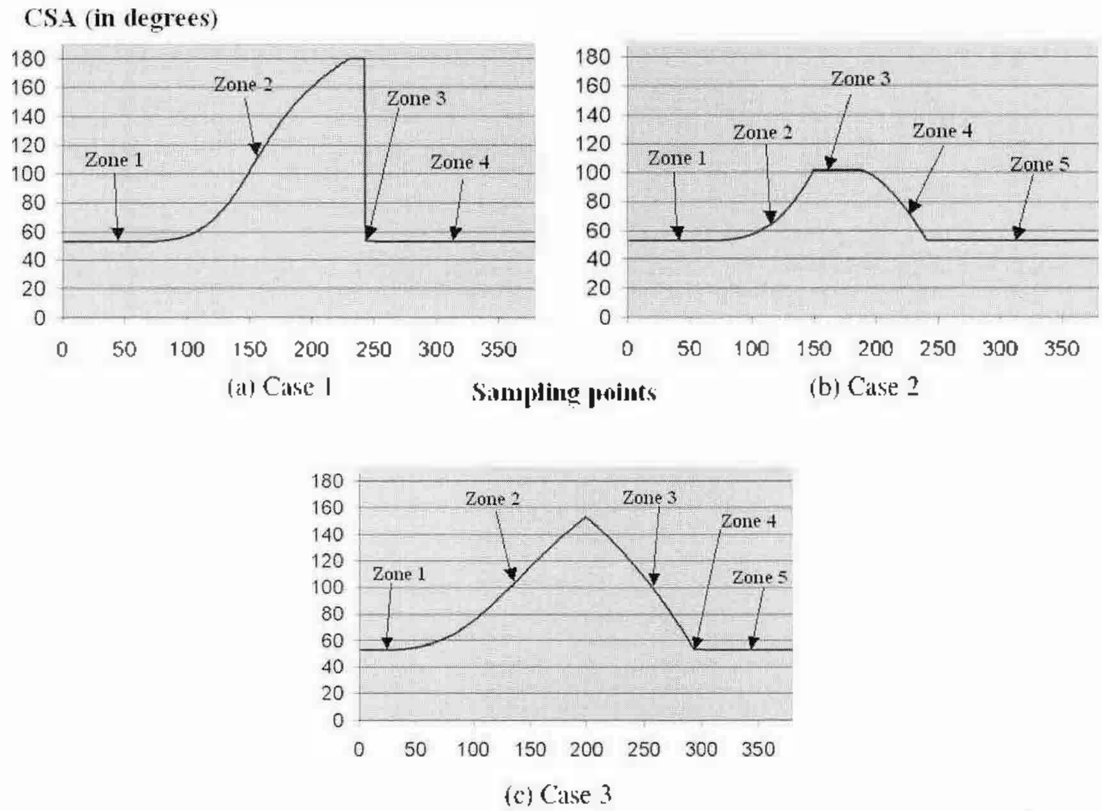

Fig. 19. Examples for modeling the cutter swept angle for different corner cases.

It can be observed from Fig. 19(c) that CSA rises steadily to a maximum of about 150° and then slides down gently without exhibiting a constant CSA zone. The overall CSA plot is stretched horizontally. In comparison, the maximum CSA obtained in Fig. 19(c) is greater than that in Fig. 19(b). It is because, after joining a fillet in the previous tool center path, the stock material left behind for the current filleted tool path to remove becomes greater.

Fig. 20 shows the experimental cutting force and simulated CSA result for the line-line corner for the mentioned three cases. The first, second and third rows of the figure represent the result of Case 1, Case 2 and Case 3 for line-line corner respectively. The cutting force result is shown in the first two columns. The third column shows the simulated CSA result by using the proposed CSA modeling scheme. The experimental settings for column 1 and column 2 are denoted by parameters Pa and Pb respectively. Pa = (Spindle speed = 1500 rpm, Feedrate = 100 mm/min), Pb = (1200 rpm, 150 mm/min). It can be observed from the figure that the inherent shape of cutting force graphs is directly proportional to the simulated CSA graphs. The higher the metal removal rate, the more similar is the shape between cutting force graphs and CSA graphs. Similarly, the experimental and simulated result for CCW arc-CW arc corner of an included angle of 53 degrees (Fig. 18(b)) is plotted in Fig. 21. The cutting force result also agrees with the previous CSA simulated result and analysis.

It should be noted that the plotted results for these three exemplary cases for either line-line corner or CCW arc- CW arc corner cannot fully represent the other cases because of the following four factors. Firstly, different tool path geometries can alter the shape of the initial and final zones of the figures. Secondly, different

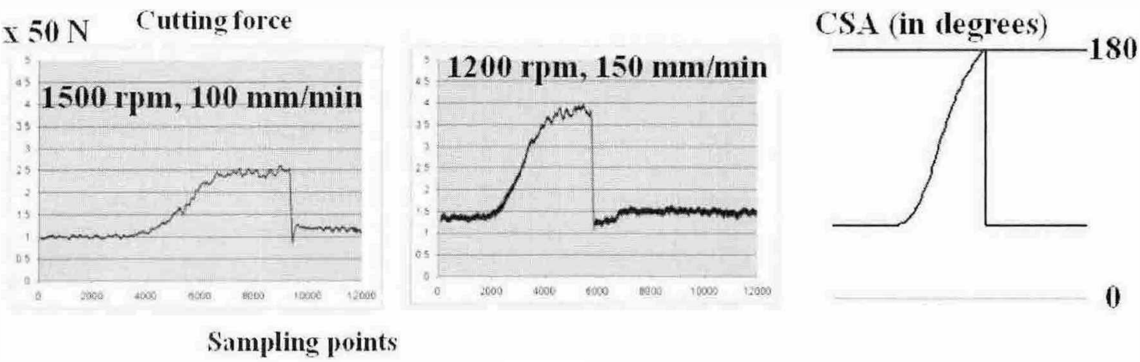

Cutting force and simulated CSA result for corner (a) of Case 1

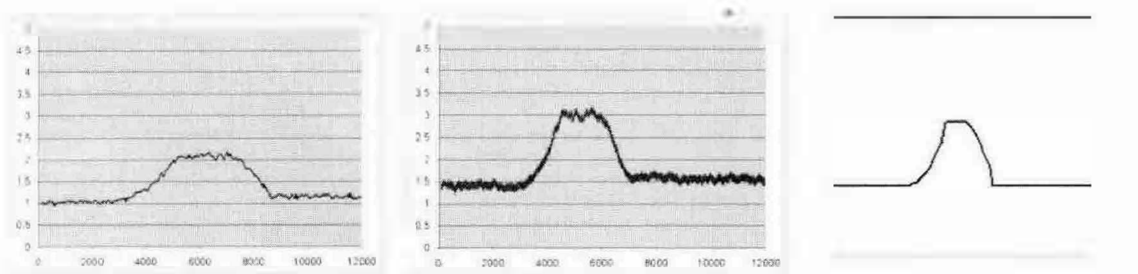

Cutting force and simulated CSA result for corner (a) of Case 2

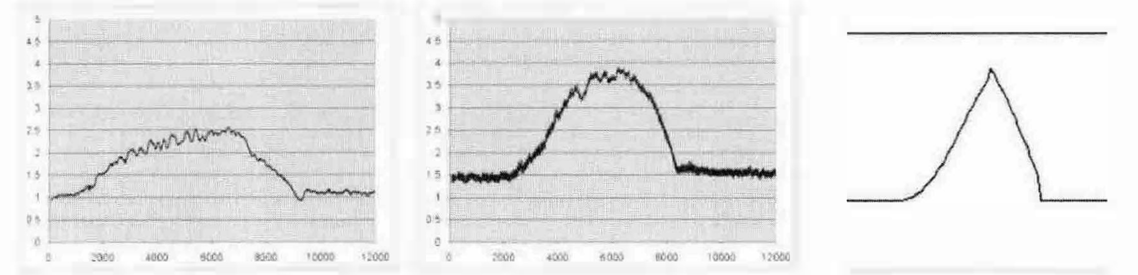

Cutting force and simulated CSA result for corner (a) of Case 3

Fig. 20. Experimental result for line-line corner cases.

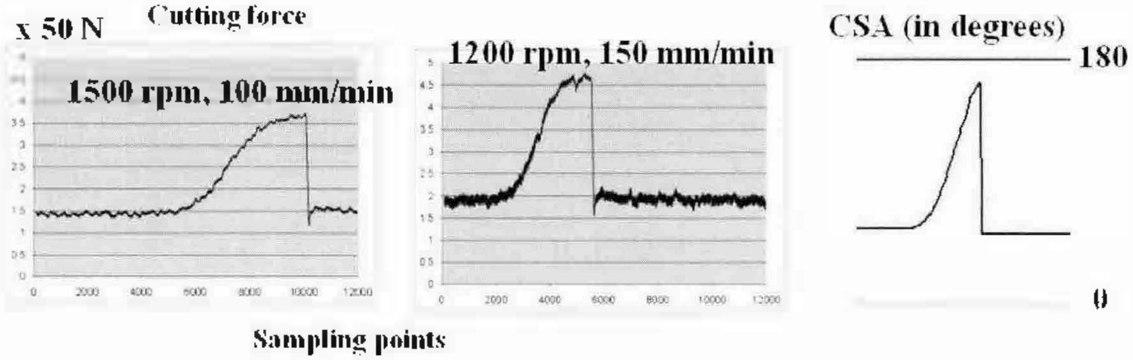

Cutting force and simulated CSA result for corner (f) of Case 1

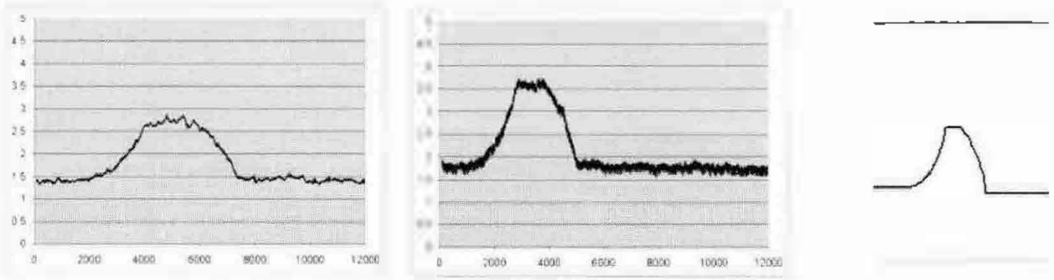

Cutting force and simulated CSA result for corner (f) of Case 2

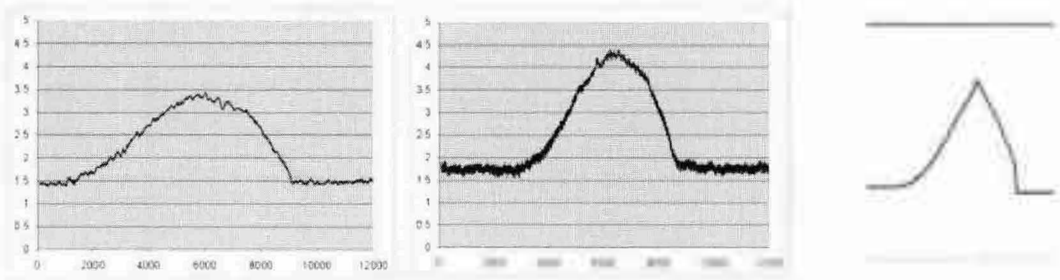

Cutting force and simulated CSA result for corner (f) of Case 3

Fig. 21. Experimental result for CCW arc-CW arc corner cases.

tool path stepover distance can shift the CSA curve upwards or downwards. Thirdly, different specified fillet radius at the tool centre path corner can narrow or widen the middle part of the CSA curve. Fourthly, different corner angles can cause different extent of material accumulation. For example, a corner of acute angle has more corner material than that of an obtuse angle.

By using CSA simulated graph, CSA data at different locations for a concerned corner tool path portion can be obtained. If the maximum magnitude for the collected CSA data exceeds an acceptable CSA angle specified by the users, this information implies that the cutting force encountered during this corner cutting will exceed the recommended limit. Adverse cutting effect such as machine chatter, tool deflection or even cutter breakage may occur. To suppress the maximum encountered cutting force during this corner cutting, two distinct approaches as mentioned in section 2 are recommended. For approach 1, an adaptive control system installed on a CNC machine is used to decelerate the cutter motion before corner cutting. However, this approach is at the expense of a lower machining efficiency since the effective corner cutting feed rate will be significantly lower than the programmed feedrate. As for approach 2, a modification of tool path geometry proposed by Iwabe *et al.* [5] and Tsai *et al.* [12] can be used. This approach has been recognized to be effective for corner cutting [4]. However, the application of Iwabe-Tsai's proposed corner-looping cut technique is limited to simple corners formed by two straight line segments. Recently, the technique has been further improved and extended to apply for more complex corner shapes by Choy *et al.* [1].

5. Conclusions

This work addresses the issue of drastic change of cutter resistance when milling concave corners. The instantaneous cutter swept angle CSA is considered as a suitable parameter for studying chip load. A classification based on a combination of different corner boundary geometries and tool centre path geometries is established. Based on this classification, a detailed analysis of CSA at different intermediate stages of corner cutting is conducted. The mathematical equations for evaluating CSA in different cutting zones are also deduced.

Graphical plotting of the CSA values calculated by the derived equations can be used to explain the severe fluctuation of cutting forces in cornering cut. Cutting force measuring experiments have verified the direct correlation between the CSA and the actual cutting resistance incurred. The established CSA modeling scheme will be an important tool for supporting investigation of the problems of cornering cut. Furthermore, possible solutions for solving corner-cutting problems have also been reviewed. One distinct advantage of modeling the CSA is to facilitate the optimization of milling conditions by saving actual machining cost and time.

Acknowledgements

The authors express their gratitude to the Department of Mechanical Engineering of the University of Hong Kong for providing all the software and hardware facilities as required in this research.

References

[1] Choy, H. S. and Chan, K. W. (2002), A corner-looping based tool path for pocket milling, *Computer-Aided Design*, **35**(2), 155-166.

[2] Fussell, B. K., Jerard, R. B. and Hemmett, J. G. (2001), Robust feedrate selection for 3-Axis NC machining using discrete models, *Journal of Manufacturing Science and Engineering*, Transactions of the ASME, **123**, 214-224.

[3] Hinduja, S., Ma, Y. S. and Barrow, G. (1995), Determination of radial width of cut and cutting modes in milling, *International Journal of Machine Tools & Manufacture*, **35**(1), 689-699.

[4] Hinduja, S., Roaydi, A., Philimis, P. and Barrow, G. (2001), Determination of optimum cutter diameter for machining 2-1/2 D pockets, *International Journal of Machine Tools & Manufacture*, **41**, 687-702.

[5] Iwabe, H., Fujii, Y., Saito, K. and Kishinami, T. (1989), Study on corner cut by end mill - analysis of cutting mechanism and new cutting method at inside corner, In Japanese, *Journal of Japan Society of Precision Engineering*, **55**(5), 841-846.

[6] Kline, W. A., Devor, R. E. and Lindberg, J. (1982), Prediction of cutting forces in end milling with application to cornering cuts, *International Journal of Machine Tool Design and Research*, **22**, 7-22.

[7] Kramer, T. R. (1992), Pocket milling with tool engagement detection, *Journal of Manufacturing Systems*, **11**(2), 114-123.

[8] Spence, A. D. and Altintas, Y. (1994), A solid modeller based milling process simulation and planning system, *Journal of Engineering for Industry*, **116**, 61-69.

[9] Stori, J. A. and Wright, P. K. (2000), Constant engagement tool-path generation for convex geometries, *Journal of Manufacturing Systems*, **19**(3), 172-184.

[10] Tarng, Y. S. and Shyur, Y. Y. (1993), Identification of radial depth of cut in numerical control pocketing routines, *International journal of Machine Tools & Manufacture*, **33**(1), 1-11.

[11] Tlusty, J., Smith, S. and Zamudio, C. (1990), New NC routines for quality in milling, *Annals of the CIRP*, **39**(1), 517-521.

[12] Tsai, M. D., Takata, S., Inui, M., Kimura, F. and Sata, T. (1991), Operation planning based on cutting process models, *Annals of CIRP*, **40**(1), 95-98.